SUPPLEMENTARY INFORMATION

RADIAL SAMPLE PRECONCENTRATION

Brent Scarff[1], Carlos Escobedo[1], and David Sinton[1,]*

[1] Mechanical Engineering, The University of Victoria, Victoria, British Columbia, Canada

* e-mail: dsinton@uvic.ca

In the article, a radial sample preconcentration strategy is presented including numerical and experimental results. The numerical model is based on the Poisson-Nernst –Planck and Navier-Stokes equations. The details on the development of the simulation model are presented here, followed by experimental details on the chip assembly and an analysis of dispersion characteristics of injected plugs.

S-1.1 Modeling Nanochannel Transport within a Nafion Nanoporous Membrane

Nafion® is a perfluoronated sulfonic membrane composed of a fluorocarbon backbone and sulfonic acid groups SO_3H which dissociate into SO_3^- and H^+ in the presence of water. A hydrated Nafion membrane can be considered as a capillary network where the sulfonic groups are uniformly distributed at the pore surface giving a constant surface charge $\sigma_{surface}$ [1].

To model the electric double layer (EDL) the Stern-Gouy-Chapman model is adopted where the Stern layer is taken as the effective pore boundary. This assumption necessitates the use of an effective surface charge σ where $\sigma < \sigma_{surface}$ since the positive charge in the Stern layer will screen some of the surface charge lowering its value at the outer Helmholtz plane [1-2]. Within the literature various values of surface

charge density exist varying from approximately -200mC/m^2 to -500mC/m^2 [1]. In the present model given the effective membrane conductivity is reduced at lower membrane thicknesses [3-4] there is some uncertainty as to the value of σ. A value of -300mC/m^2 was found to provide a good fit to experimental data, was within the range of previously reported values and was applied in this work. It was assumed that the membrane hydration does not vary and the effect of varying water content on pore size is negligible. A constant radius of $r_p = 2.5\ nm$ was assumed [5-6].

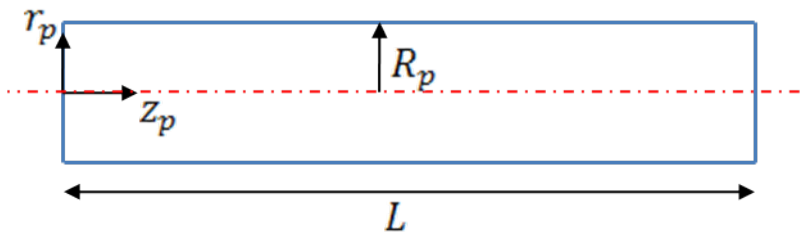

Fig. S1 Schematic of the assumed pore geometry employed in the computational model and the coordinate system.

First the equilibrium concentration and potential profiles within one pore (Fig. S1) are established, the initial conditions for the membrane are then deduced by up scaling the model for a given porosity. The distribution of ions within the diffuse part of the double layer in a charged capillary is given by the Boltzmann distribution

$$c_i(z_P) = c_i^0 \exp\left(-\frac{z_i e\psi(r_p, z_p)}{kT}\right) \qquad \text{S-1}$$

Where e, k and T are the elementary charge, Boltzmann constant and temperature respectively. $\psi(r_p, z_p)$ is the field induced by the EDL and c_i^0 is the concentration where mathematically $\psi(r_p, z_p) = 0$.

To relate the channel potential with the variation in concentration, Poisson's equation is employed

$$\nabla^2\psi(\mathrm{r_p},\mathrm{z_p}) = -\frac{1}{\epsilon_0\epsilon_r}\sum_{i=1}^{N} z_i F c_i \qquad \text{S-2}$$

Expanding terms in the cylindrical coordinate system gives

$$\frac{1}{r_p}\frac{\partial}{\partial r_p}\left(r_p\frac{\partial\psi(\mathrm{r_p},\mathrm{z_p})}{\partial r_p}\right)+\frac{\partial^2\psi(\mathrm{r_p},\mathrm{z_p})}{\partial {z_p}^2} = -\frac{1}{\epsilon_0\epsilon_r}\sum_{i=1}^{N} z_i F c_i \qquad \text{S-3}$$

where σ is the surface charge density $[C/m^2]$ and ϵ_r is the relative permittivity of hydrated Nafion which will be assumed constant and equal to 45 [7]. In long narrow capillaries ($L >> R_p$) the axial variation in potential is negligible compared with the radial variation and the axial derivative $\left(\frac{\partial^2}{\partial z^2}\right)$ can be neglected. Substituting the concentration distribution S-1 into equation S-3 gives the Poisson-Boltzmann equation

$$\frac{1}{r_p}\frac{\partial}{\partial r_p}\left(r_p\frac{\partial\psi}{\partial r_p}\right) = -\frac{1}{\epsilon_0\epsilon_r}\sum_{i=1}^{N} z_i F c_i^0 \exp\left(-\frac{\mathrm{z_i} e\psi}{kT}\right) \qquad \text{S-4}$$

Appropriate boundary conditions specify symmetry at the centerline (z = 0) and field flux at the charged surface

$$\frac{d\psi}{dr_p} = 0, \qquad r_p = 0$$
$$\frac{d\psi}{dr_p} = -\frac{\sigma}{\epsilon_0\epsilon_r}, \qquad r_p = \mathrm{R_p} \qquad \text{S-5}$$

Given the assumption of constant surface charge the model can be reduced to one dimension by taking area averages of potential and concentration distributions within the pores. The area average of a function within a cylindrical pore is defines as

$$\langle f \rangle = \frac{2}{{R_p}^2} \int_0^{R_p} f(r_p) r_p dr_p \qquad \text{S-6}$$

For the 1D model an expression is required to include the effect of surface charge (σ). In the 1D sense the effect is the same as a fixed charge concentration within the pore. Such an expression can be obtained by integrating equation S-3 with boundary conditions specified in S-5. This reduces to an expression for overall electroneutrality

$$\sum_{i=1}^{N} z_i \langle c_i \rangle + \frac{2\sigma}{F R_p} = 0 \qquad \text{S-7}$$

The second term on the LHS of equation S-7 can be thought of as the fixed charge concentration and is how the surface charge density enters the 1D model.

S-1.1.1 Summary of Initial Conditions

Equation S-4 was solved numerically in Matlab using the BVP4C command to provide concentration and potential profile distributions. The potential at the wall (i.e. at the stern layer) was taken as the zeta potential (ζ) of the pore and used in subsequent pore velocity calculations. Results were subsequently numerically integrated using the trapezoidal method in accordance with equation S-6 to obtain area average values. Only solution of the co-ion species concentration field is required while the condition of electroneutrality (equation S-7) is used to solve for the counter-ion distribution.

S-1.2 Hydrodynamics within Nanochannels

Under the influence of an applied field the electrostatic potential at any point in the problem domain can be decomposed into a linear superposition [8]

$$\Phi(\mathrm{r},\mathrm{z}) = \phi(z) + \psi(r,z) \qquad \text{S-8}$$

Where $\phi(z)$ is the field due to an applied voltage and $\psi(r,z)$ is the potential due to the EDL. Newtonian laminar fluid flow with constant properties in a narrow cylindrical capillary is governed by the Navier-Stokes and continuity equations in cylindrical coordinates as follows

$$-\frac{\partial P}{\partial z} + \mu \frac{1}{r_p}\frac{\partial}{\partial r_p}\left(r_p \frac{\partial u}{\partial r_p}\right) - \sum_{i=1}^{N} z_i F c_i \frac{\partial \phi}{\partial z} = 0 \qquad \text{S-9}$$

$$\frac{\partial u}{\partial r_p} = 0 \qquad \text{S-10}$$

With boundary conditions

$$u(R_p) = 0; \qquad \left.\frac{\partial u}{\partial r_p}\right|_{r_p=0} = 0 \qquad \text{S-11}$$

where P is the induced pressure required to maintain system continuity and μ is the viscosity assumed to be constant and equal to $1 \times 10^{-3}\, kg/m \cdot s$ within the pore. Equation S-9 has the electrical body force included accounting for the effect of the externally applied electric field. To avoid solving the full Navier-Stokes equations the analytical solution to the velocity profile in a capillary will be used. The velocity profile is a linear superposition of electroosmotic and induced pressure driven flows

$$u(r_p) = -\frac{1}{4\mu}\frac{dP}{dz_p}\left({R_p}^2 - {r_p}^2\right) + \frac{\epsilon_0 \epsilon_r \zeta}{\mu}\left(1 - \frac{\psi}{\zeta}\right)\frac{d\phi}{dz_p} \qquad \text{S-12}$$

The area average of this equation can be taken with the result

$$\langle u_p \rangle = -\frac{{R_p}^2}{8\mu}\frac{dP}{dz_p} + \frac{\epsilon_0 \epsilon_r \zeta}{\mu}(1 - G)\frac{\partial \phi}{\partial z_p} \qquad \text{S-13}$$

where, as per Levine et al.[9] G is defined as

$$G = \frac{2}{\zeta {R_p}^2}\int_0^{\mathrm{Rp}} r_p \psi(r_p) dr_p \qquad \text{S-14}$$

The zeta potential is a function of the local concentration and thus will vary between the nanofluidic and microfluidic regimes. Additionally, the concentration at the interface between these two domains varies significantly on account of the exclusion enrichment effect. To facilitate numerical simulation of this dynamic process the factor $\zeta(1-G)$ is calculated over a range of concentrations in the nano regime. Within the microchannel the factor $\frac{1}{\zeta h}\int_{-\frac{h}{2}}^{\frac{h}{2}} \psi(z)\, dz$ is calculated (see Table S2 for equations and domain details). Data can then be fit to a curve of the form [10]

$$\zeta_{Effectuve} = a_1\left(1-\tanh\left(-\frac{\ln(\lambda(x))}{a_2}+a_3\right)\right) \qquad \text{S-15}$$

where pH is assumed constant and the Debye length (λ) has been introduced as the concentration dependent parameter. The resultant variation in the effective ζ with concentration can be seen in Fig. S2 for the microchannel and nanopore.

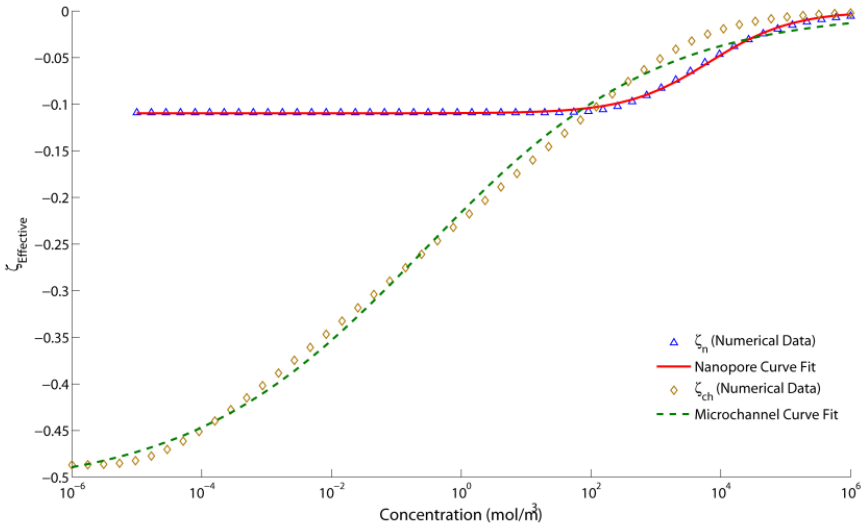

Fig. S2 Effective zeta potential over a range of concentrations at T = 298K for $\sigma_{ch} = 150\ C/m^2$, $\sigma_m = 300\, C/m^2$, $h_m = 20\mu m$, $r_p = 2.5nm$

S-1.3 Species Transport

Within the microchannel domain, governing equations for the electric field and velocity profiles were developed as described in the previous section making careful note of the change in coordinate system. The overall problem domain (depicted in Fig. 2 in the main article) was approximated as two infinite parallel discs with varying height between the microchannel domain (h_{ch}) and membrane domain (h_m), here $h_{ch} = 20\mu m$ and $h_m = 50nm$. The variation in height and domain properties was modeled as a smoothed Heaviside function transitioning over a length of $5\mu m$. The $V_{Effective}$ boundary condtion at the central axis is of the form $V\left(1 - e^{-\frac{t}{0.65s}}\right)$, where the short time constant was added to avoid instabilities at the onset of the simulation.

An expression for species transport within a dilute solution is given by the conservation equation

$$\frac{\partial c_i}{\partial t} + \nabla \cdot \mathrm{J} = 0 \qquad \text{S-16}$$

where the flux J is given by

$$J = uc_i - \nu_i z_i F \frac{\partial \phi}{\partial r} c_i - D_i \frac{\partial c_i}{\partial r} \qquad \text{S-17}$$

where c_i, ν_i, z_i, and D_i are the concentration, mobility, valence number and diffusion coefficient respectively for the i^{th} ion. F is Faraday's constant u and $\frac{\partial \phi}{\partial r}$ are the velocity and electric field strength respectively. Tabulated diffusion data was used to calculate the ion mobilities using Einstein's relation $\left(\nu_i = \frac{D_i}{RT}\right)$.

A binary symmetric buffer is assumed providing two dominant ionic species (i = 1,2) along with a negatively charged tracer, or analyte of interest (i = 3). As per

Pennathur and Santiago [11] the dilute binary solution approximation is still valid for low concentrations of tracer species. Integrating the expression over the channel height

$$\int_{-\frac{h}{2}}^{\frac{h}{2}} J\, dz = \int_{-\frac{h}{2}}^{\frac{h}{2}} u_r\, c_i dz - \nu_i z_i F \frac{\partial \phi}{\partial r}\left(\int_{-\frac{h}{2}}^{\frac{h}{2}} c_i\, dz\right) - D_i \int_{-\frac{h}{2}}^{\frac{h}{2}} \frac{\partial c_i}{\partial r} dz \qquad \text{S-18}$$

In this reference frame the area average function is defined as

$$\langle g \rangle = \frac{1}{h}\int_{-\frac{h}{2}}^{\frac{h}{2}} g(r,z) dz \qquad \text{S-19}$$

Expressing S-17 in terms of area averaged quantities

$$\langle J \rangle = h\langle u \rangle \langle c_i \rangle - \nu_i z_i F \frac{\partial \phi}{\partial r} h\langle c_i \rangle - D_i h \frac{\partial \langle c_i \rangle}{\partial r} \qquad \text{S-20}$$

Two simplifications have been made in equation S-20, first the convective term has been simplified $\langle u c_i \rangle = \langle u \rangle \langle c_i \rangle$ which equates to neglecting axial dispersive terms [5]. The simplification is justified by the work of Bernardi and Verbrugge [6] who showed within a Nafion membrane the velocity is essentially constant. The second simplification is the diffusion term $\frac{\partial h\langle c_i \rangle}{\partial r} = h\frac{\partial \langle c_i \rangle}{\partial r}$. Again, this simplification is justified in the case that $\left|\frac{dh}{dr}\right| \ll 1$ which is the case here.

Poisson's equation is again used to relate the channel potential with the concentration distribution, in the modified coordinate system

$$\frac{1}{r}\frac{\partial}{\partial r}\left(r\frac{\partial \phi}{\partial r}\right) + \frac{\partial^2 \psi}{\partial z^2} = -\frac{F}{\epsilon_0 \epsilon_r}\sum_{i=1}^{N} z_i c_i \qquad \text{S-21}$$

Taking the area average of S-21 with boundary conditions

$$\frac{d\psi}{dz} = 0, \qquad z = 0$$
$$\frac{d\psi}{dz} = -\frac{\sigma_{ch}}{\epsilon_0 \epsilon_r}, \qquad z = \frac{\mathrm{h}}{2} \tag{S-22}$$

Results in

$$\frac{1}{r}\frac{\partial}{\partial r}\left(r\frac{\partial \phi}{\partial r}\right) = -\frac{\mathrm{F}}{\epsilon_0 \epsilon_r}\sum_{i=1}^{N} z_i \langle c_i \rangle + \frac{2\sigma_{ch}}{h_{ch} F} \tag{S-23}$$

Equation S-23 relates the radial variation in concentration to the field strength.

S-1.4 Relations to Porous Domain

Concentration within a nanopore is related to the membrane concentration via the porosity ϵ_w. Likewise from continuity the velocity within a pore can be related to the superficial velocity, that is the velocity through the membrane assuming no porous structure existed. The expressions relating the microchannel domain with the membrane and pore domain are

$$c_m = \epsilon_w c_p,$$
$$q'_{ch} = u_{ch} h_{ch} = u_m h_m = q'_m \tag{S-24}$$
$$Q_m = Q_p \epsilon_w = u_p A_p \epsilon_w$$

where $c_m$and c_p are the concentrations in the pore and membrane respectively and u_{ch}, u_m and u_p are the velocities in the channel, membrane and pore respectively. q'_{ch}, q'_m, Q_m and Q_p are the per unit depth and total flow rates within the channel, membrane and pore. A_p is the cross sectional area of the cylindrical pore.

S-1.5 Summary of Model Properties

In this section the properties and final form of the equations implemented in the commercial multiphysics software Comsol 3.5 are detailed. Justification for the concentration values employed is also presented.

S-1.5.1 Electrolyte Properties

In experimental trials 10mM TAE buffer at pH = 8.1 is used as the background electrolyte (BGE). 10 mM TAE consists of 20 mM of Tris base (pKa = 8.1), 10 mM of Acetic Acid (pKa = 4.8) and 0.25 mM of EDTA. EDTA is used to sequester divalent cations that may interfere with biological studies and will be neglected in the model. For a partially ionized univalent weak electrolyte in dilute solution the effective mobility (ν_{eff}) [12] is given by

$$\nu_{eff} = \alpha\nu \qquad \text{S-25}$$

Where α is the degree of dissociation and ν is the fully ionized mobility.

The Henderson-Hasselbach equation applied to the acid dissociation equilibrium $HA \rightleftharpoons H^+ + A^-$ gives an indication as to the magnitude of α

$$pH = pKa + log\frac{[A^-]}{[HA]} \qquad \text{S-26}$$

Where $[A^-]$ is the concentration of the conjugate base and $[HA]$ is the concentration of the acid. In the case of Acetic Acid $pKa \ll pH$ the ratio $\frac{[A^-]}{[HA]}$ is large and it can be assumed that the acid is in its fully ionized state ($\alpha = 1$). In the case of a base the equilibrium is $BH^+ \rightleftharpoons B + H^+$ and equation S-26 is modified as follows

$$pH = pKa + log\frac{[B]}{[BH^+]} \quad \text{S-27}$$

For the case where $pH \approx pK_a$ as with the case of Tris base the ratio $\frac{[B]}{[BH^+]} \approx 1$ and equal parts base and conjugate base are present giving $\alpha = 0.5$. Concentrations of positive and negative ions can thus both be taken as 10 mM (10 mol/m^3).

S-1.5.2 Equations and Parameters

Tables S1 and S2 break down the model and present relevant domain equations, parameters and initial conditions.

Diffusion parameters for the Acetate ion (D^-) and Tris Base (D^+) are based on refs [13-14]. The fluorescein tracer diffusion coefficient (D_{Tracer}) is based on ref. [15]. A factor of 0.5 was applied for the diffusion coefficients in the membrane to account for the tortuosity in the membrane. The value of surface charge density was taken by halving the Nafion surface charge density (effectively averaging surface charge of the top PDMS surface and bottom Nafion surface).

Table S1: Initial Conditions

Microchannel	**Membrane**
$c_i = c_0$	$c_2 = \epsilon c_p$ $c_1 = c_2 + \frac{2\epsilon_w \sigma}{Fr_0}$
$\phi = 0$	$\phi = \epsilon_w \psi_p$
$P = 0$	$P = 0$

Table S1: Model Equations by Domain

Parameter	**Microchannel**	**Membrane**	**Nanopore**
ϕ	$\frac{1}{r}\frac{\partial}{\partial r}\left(r\frac{\partial \phi}{\partial r}\right) = -\frac{F}{\epsilon_0\epsilon_r}\sum_{i=1}^{N} z_i\langle c_i\rangle + \frac{2\sigma_{ch}}{h_{ch}F}$	$\frac{1}{r}\frac{\partial}{\partial r}\left(r\frac{\partial \phi}{\partial r}\right) = -\frac{F}{\epsilon_0\epsilon_r}\sum_{i=1}^{N} z_i\langle c_i\rangle + \frac{2\epsilon_w\sigma_{eff}}{{R_p}^2F}$	–
u	$u_{ch} = \frac{1}{2\mu}\left(z^2 - \frac{h^2}{4}\right)\frac{dP}{dr} + \frac{\epsilon_0\epsilon_r\zeta}{\mu}\left(1-\frac{\psi}{\zeta}\right)\frac{d\phi}{dr}$ $\langle u_{ch}\rangle = -\frac{h^2}{12\mu}\frac{dP}{dr} + \frac{\epsilon_0\epsilon_r\zeta}{\mu}(1-G_{ch})\frac{d\phi}{dr}$ $G_{ch} = \frac{1}{\zeta h}\int_{-\frac{h}{2}}^{\frac{h}{2}}\psi(z)dz$	$\langle u_m\rangle = \epsilon_w\langle u_p\rangle A_p h_m$	$u_p = \frac{1}{r\mu}\left({R_p}^2 - {r_p}^2\right)\frac{dP}{dz_p} + \frac{\epsilon_0\epsilon_r\zeta}{4\pi\mu}\left(1-\frac{\psi}{\zeta}\right)\frac{d\phi}{dz_p}$ $\langle u_p\rangle = \frac{{R_p}^2}{8\mu}\frac{dP}{dz_p} + \frac{\epsilon_0\epsilon_r\zeta}{4\mu}\left(1-G_p\right)\frac{d\phi}{dz_p}$ $G_p = \frac{2}{\zeta {R_p}^2}\int_0^{R_p} r_p\psi(r_p)dr_p$
c_i	$\frac{d\langle c_i\rangle}{dt} + \nabla\cdot\langle J\rangle = 0$ $\langle J\rangle = h\langle u_{ch}\rangle\langle c_i\rangle - \nu_i z_i F\frac{d\phi}{dr}h\langle c_i\rangle - D_{i,ch}\,h\frac{d\langle c_i\rangle}{dr}$	$\frac{d\langle c_i\rangle}{dt} + \nabla\cdot\langle J\rangle = 0$ $\langle J\rangle = h\langle u_m\rangle\langle c_i\rangle - \nu_i z_i F\frac{d\phi}{dr}h\langle c_i\rangle - D_{i,m}\,h\frac{d\langle c_i\rangle}{dr}$	$\frac{1}{r_p}\frac{\partial}{\partial r_p}\left(r_p\frac{\partial\psi}{\partial r_p}\right) = -\frac{1}{\epsilon_0\epsilon_r}\sum_{i=1}^{N} z_i F c_i^0 \exp\left(-\frac{\mathrm{z_i}e\psi}{kT}\right)$
P	$\nabla\cdot\langle u_{ch}\rangle = 0$	$\nabla\cdot\langle u_m\rangle = 0$	–

S-1.6 Equivalent Circuit Model for Determining Effective Voltage

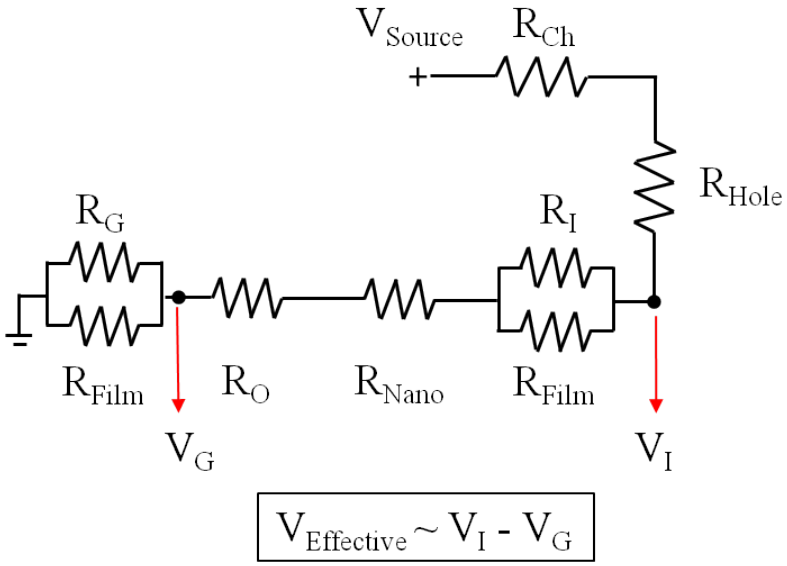

Fig. S3 Equivalent circuit model. R_{Ch} is the upper channel resistance, R_{Hole} is the punched hole resistance, R_I is the inner chamber resistance, R_{Film} is the Nafion film resistance, R_{Nano} is the active nano membrane resistance, R_O is the outer radial channel resistance and R_G is the resistance of the channel leading to ground.

For experimental trials the source voltage is on the order of 200-1000V, however the effective voltage difference across the preconcentration layer will vary from this applied voltage due to the various resistances within the microfluidic network. To estimate the effective voltage an equivalent wiring diagram was used (Fig. S3) where resistances are calculated in a similar manner to Ref.[16] using the relationship

$$R_i = \frac{1}{\kappa} \times \frac{L_i}{A_i} \qquad \text{S-28}$$

Where R_i is the resistance, κ, L_i and A_i are the conductivity, path length and cross sectional area respectively. The conductivity of the BGE was measured using a conductivity meter as 488 $\mu S/cm$. The currents within the inner radial chamber and the grounding channel have two

paths through which to travel, the bulk solution or the Nafion film. The resistance here is calculated as an equivalent resistance of two resistors in parallel. The same equivalence is not performed for the outer radial channel since this is on the enrichment side of the membrane and thus the solution will see an increase in conductivity and should dominate as the preferential current path. The voltage difference across the microfluidic network can be calculated using a voltage divider formula

$$V_I = \frac{R_{equiv,I} + R_{Nano} + R_O + R_{equiv,G}}{\sum R_i} \times V_{Source} \qquad \text{S-29}$$

and likewise for V_G

$$V_G = \frac{R_{equiv,G}}{\sum R_i} \times V_{Source} \qquad \text{S-30}$$

As the depletion region develops within the radial chamber one would expect V_I to increase as the conductivity within the solution drops. Through modeling simulations the conductivity was estimated to decrease by a factor of 200 within the depletion region. The effective voltage, $V_{Effective}$, was calculated for the initial experimental condition where the radial chamber is filled with buffer (high conductivity) solution and the end condition where the radial chamber is filled with the depleted buffer (low conductivity) solution. The conductivity of Nafion is known to be suppressed in recast films[4] so κ_{Nafion} was used as a fitting parameter within the model with the value being determined as $\kappa_{Nafion} = 0.00145\, S/cm$. Such a value is in line with results reported within Ref. [4] for nanometer thick films at room temperature. With given values and a source voltage of 400V the voltage varied little between the non-depleted (~94 V) and depleted (~95 V) times. An accurate fit to experimental data could thus be gained by applying a constant voltage boundary condition $V_{Effective}$ taken as 95V.

S-1.7 Device Fabrication

The microfluidic chip was fabricated in poly-dimethylsiloxane (PDMS) (Sylgard, Dow Corning Corporation, Midland, MI) using established soft-lithography techniques.[17-18] Inlet and outlet holes were punched in the PDMS at the reservoir locations, an additional small diameter hole was punched at the center of the circular chamber using a 25 gauge needle (ID = $241.3\mu m$) with the end ground flat. For the protein experiments the PDMS chip was washed with isopropyl alcohol and dried prior to being treated in a plasma cleaner (Harrick PDC 32-G) for 60 seconds to ensure a hydrophilic surface condition. Following plasma treatment the chip and substrate were exposed to a BSA blocking solution for one hour. After blocking, the chip was brought into contact with the Nafion® coated substrate and clamped between two PMMA plates. Fig. S3 shows the assembly of the microfluidic chip. For difficult geometries a drop of the working solution was placed on the Nafion prior to placing the PDMS chip on top, this allowed the fluid to fill difficult spaces, assembly then commenced as normal. Any entrapped air bubbles were removed using the vacuum assisted filling techniques detailed in Ref. [19]. Once filled chips sat for a minimum of 20 minutes to allow the Nafion to hydrate.

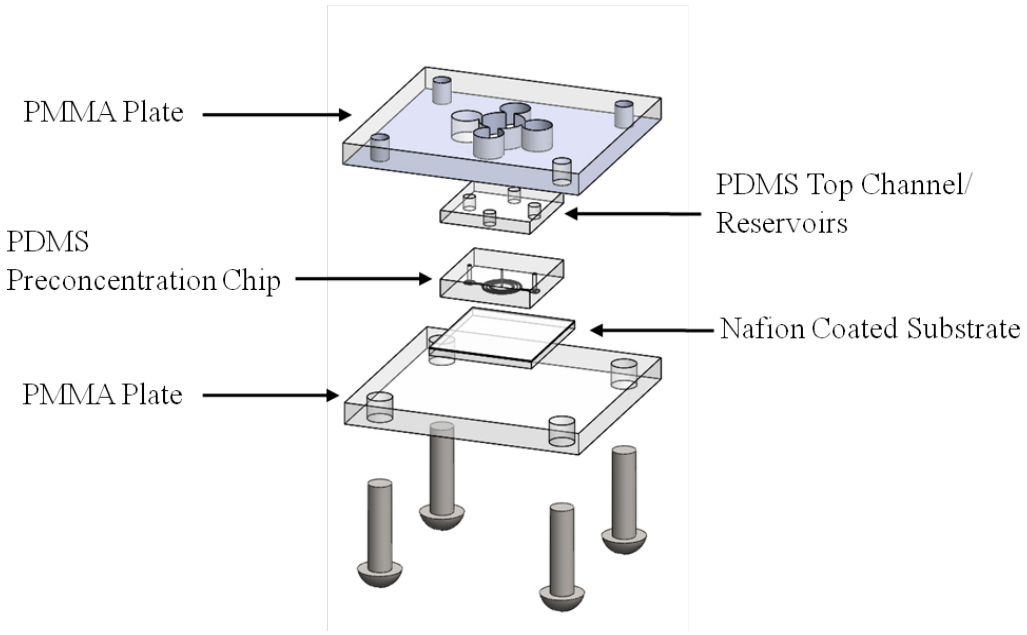

Fig. S3 Chip Assembly

S-1.8 Dispersion of Injected Plugs

Within the present electrode scheme the sample was seen in several cases to disperse and split in two once injected into the top microfluidic analysis layer. Due to the variance in the effective zeta potentials (see Fig. S2) the flow rate induced in the nanopores is less than the flow rate in the microchannel due to the high electro-viscous retarding forces seen in the nanopores where dimensions approach the Debye length. The result is an induced back pressure at the micro-nano interface that builds with time creating a pressure driven component to the flow field [10]. Once the concentrated plug reaches the microfluidic analysis layer the induced pressure driven flow drives the plug in the channel causing the dispersive effects typical of these types of flows. To avoid these secondary pressure driven flows a voltage switching scheme would be implemented in practice. In practice this back-pressure would be avoided by floating the ground channel and effectively turning off the concentration mechanism once the sample is in the analysis channel.

Of note in the case of the finned chamber is the reduced dispersion of the injected plug.

Fig. 7a of the main text shows the concentrated plug loses little of its concentration increase while traveling through the channel. This can be explained by looking at the expression for flow rate within the microchannel. Solving for the pressure term

$$-\frac{dP}{dr} = \frac{12\mu}{h^3}(Q_{ch} - hU_{EO}) \qquad \text{S-31}$$

where Q_{ch} is the flow rate in the microchannel and U_{EO} is the electroosmotic velocity. The flow rate through the membrane is the rate determining factor so assuming Q_{ch} does not vary with an increase in channel height it's seen that a reduction in the induced pressure gradient must occur to satisfy continuity. Since pressure scales to the third power of the microchannel height the effective pressure is dramatically reduced resulting in the reduced dispersion of the ejected plug.

References

1 T. Colinart, S. Didierjean, O. Lottin, G. Maranzana and C. Moyne, *Journal of the Electrochemical Society*, 2008, **155**, B244-B257.
2 Y. Yang and P. N. Pintauro, *Industrial & Engineering Chemistry Research*, 2004, **43**, 2957-2965.
3 M. W. Verbrugge and R. F. Hill, *Journal of the Electrochemical Society*, 1990, **137**, 3770-3777.
4 Z. Siroma, R. Kakitsubo, N. Fujiwara, T. Ioroi, S. I. Yamazaki and K. Yasuda, *Journal of Power Sources*, 2009, **189**, 994-998.
5 E. H. Cwirko and R. G. Carbonell, *Journal of Colloid and Interface Science*, 1989, **129**, 513-531.
6 D. M. Bernardi and M. W. Verbrugge, *Journal of the Electrochemical Society*, 1992, **139**, 2477-2491.
7 S. J. Paddison, D. W. Reagor and T. A. Zawodzinski, *Journal of Electroanalytical Chemistry*, 1998, **459**, 91-97.
8 R. F. Probstein, *Physiochemical Hydrodyanmics: An Introduction*, Wiley-Interscience, New Jersey, 1994.
9 S. Levine, J. R. Marriott, G. Neale and N. Epstein, *Journal of Colloid and Interface Science*, 1975, **52**, 136-149.
10 A. Plecis, C. Nanteuil, A. M. Haghiri-Gosnet and Y. Chen, *Analytical Chemistry*, 2008, **80**, 9542-9550.
11 S. Pennathur and J. G. Santiago, *Analytical Chemistry*, 2005, **77**, 6772-6781.

12 A. Persat, M. E. Suss and J. G. Santiago, *Lab on a Chip*, 2009, **9**, 2454-2469.
13 A. Persat, R. D. Chambers and J. G. Santiago, *Lab on a Chip*, 2009, **9**, 2437-2453.
14 D. R. Lide, ed., *CRC Handbook of Chemistry and Physics*, 2010.
15 D. Sinton, L. Q. Ren, X. C. Xuan and D. Q. Li, *Lab on a Chip*, 2003, **3**, 173-179.
16 G. B. Li, S. L. Wang, C. K. Byun, X. Y. Wang and S. R. Liu, *Analytica Chimica Acta*, 2009, **650**, 214-220.
17 D. C. Duffy, J. C. McDonald, O. J. A. Schueller and G. M. Whitesides, *Analytical Chemistry*, 1998, **70**, 4974-4984.
18 J. C. McDonald, D. C. Duffy, J. R. Anderson, D. T. Chiu, H. K. Wu, O. J. A. Schueller and G. M. Whitesides, *Electrophoresis*, 2000, **21**, 27-40.
19 J. Monahan, A. A. Gewirth and R. G. Nuzzo, *Analytical Chemistry*, 2001, **73**, 3193-3197.